Supplementary information: Gigahertz free-space electro-optic modulators based on Mie resonances

Ileana-Cristina Benea-Chelmus*
Harvard John A. Paulson School of Engineering and Applied Sciences, Harvard University, Cambridge, MA, USA

Sydney Mason
Harvard College, Cambridge, MA, USA

Maryna L. Meretska
Harvard John A. Paulson School of Engineering and Applied Sciences, Harvard University, Cambridge, MA, USA

Delwin L. Elder
University of Washington, Department of Chemistry, Seattle, WA, USA

Dmitry Kazakov
Harvard John A. Paulson School of Engineering and Applied Sciences, Harvard University, Cambridge, MA, USA

Amirhassan Shams-Ansari
Harvard John A. Paulson School of Engineering and Applied Sciences, Harvard University, Cambridge, MA, USA

Larry R. Dalton
University of Washington, Department of Chemistry, Seattle, WA, USA

Federico Capasso†
Harvard John A. Paulson School of Engineering and Applied Sciences, Harvard University, Cambridge, MA, USA

(Dated: August 11, 2021)

Abstract

Electro-optic modulators from non-linear $\chi^{(2)}$ materials are essential for sensing, metrology and telecommunications because they link the optical domain with the microwave domain. At present, most geometries are suited for fiber applications. In contrast, architectures that modulate directly free-space light at gigahertz (GHz) speeds have remained very challenging, despite their dire need for active free-space optics, in diffractive computing or for optoelectronic feedback to free-space emitters. They are typically bulky or suffer from much reduced interaction lengths. Here, we employ an ultrathin array of sub-wavelength Mie resonators that support quasi bound states in the continuum (BIC) as a key mechanism to demonstrate electro-optic modulation of free-space light with high efficiency at GHz speeds. Our geometry relies on hybrid silicon-organic nanostructures that feature low loss ($Q = 550$ at $\lambda_{res} = 1594$ nm) while being integrated with GHz-compatible coplanar waveguides. We maximize the electro-optic effect by using high-performance electro-optic molecules (whose electro-optic tensor we engineer in-device to exploit $r_{33} = 100$ pm/V) and by nanoscale optimization of the optical modes. We demonstrate both DC tuning and high speed modulation up to 5 GHz ($f_{EO,-3\ dB} = 3$ GHz) and shift the resonant frequency of the quasi-BIC by $\Delta\lambda_{res}$ =11 nm, surpassing its linewidth. We contrast the properties of quasi-BIC modulators by studying also guided mode resonances that we tune by $\Delta\lambda_{res}$ =20 nm. Our approach showcases the potential for ultrathin GHz-speed free-space electro-optic modulators.

* cristinabenea@g.harvard.edu

† capasso@seas.harvard.edu

S1. FABRICATION DETAILS

The structures discussed in this study use in part standard nanofabrication techniques used for the silicon-on-insulator platform and are complemented by a final step in which the organic active layer is applied to the structure and subsequently activated by electric field poling. The details are discussed in the Methods section of the main text, and a schematic of the fabrication protocol is provided in Fig. S1.

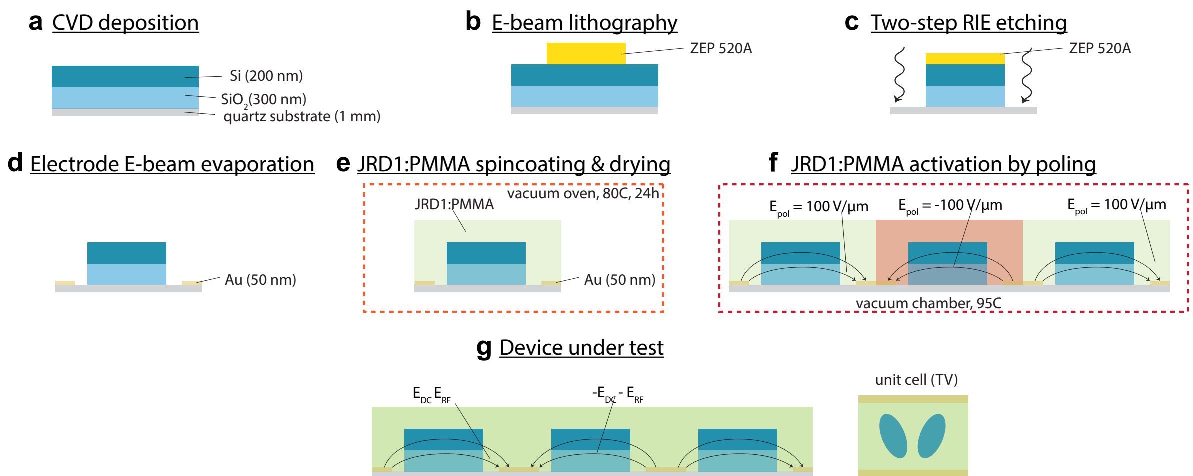

FIG. S1. **Fabrication protocol of hybrid silicon-organic modulators.** **a,** A multi-layer of amorphous silicon and silicon dioxide is deposited onto the substrate. **b,-c,** E-beam lithography is used to define the etch mask from cured ZEP 520A for the etching of the silicon and the silicon dioxide using RIE/ICP. **d,** Metallic contact electrodes are deposited via electron beam deposition. **e,** The active organic layer is applied to the nanostructures by spin coating and subsequently dried in a vacuum oven for 24 h at 80°. **f,** The organic layer is activated by electric field poling. Adjacent unit cells are poled in opposite direction, yielding an in-plane periodically poled electro-optic film, as previously introduced in Ref. [1]. **g,** While under applied driving electric field, the refractive index change is periodic across all unit cells, owing to the driving field that also switches sign from in two adjacent unit cells. CVD = chemical vapour deposition, RIE = reactive ion etching, Au = gold,

S2. OPTICAL PROPERTIES OF QUASI-BIC AND GMR RESONANCES

The structures discussed in this work support quasi-bound states in the continuum and guided mode resonances. An efficient electro-optic transduction is achieved if the strength and orientation of the optical field and the tuning DC/RF field are such that they interact strongly via the r_{33} component of the electro-optic tensor. This requires that the two fields have a strong overlap with the nonlinear material in the nearfield of the resonators and that their vectorial orientation is as parallel as possible to the field lines of the DC fields. In Fig. S2 we show various crossections of the electric fields from electromagnetic and electrostatic simulations of the optical and DC fields. A maximal electro-optic transduction driven by r_{33} between the DC/RF tuning field and the optical field is ensured by the chosen electrode orientation. Due to the sub-wavelength nature of the structures we discuss, the vectorial distribution of RF modulating fields up to 5 GHz can be approximated by the electrostatic field distribution shown in Fig. S2.

We first investigate the field distribution at three distinct locations in the plane of the array of resonators: plane A is located 50 nm below the silicon resonators, plane B is located in the center of the silicon resonators and plane C is located 50 nm above the silicon resonators in the JRD1 layer. Furthermore, we provide also the field distribution across the cross-section located at plane D. In all panels, the arrows represent the electric field vector in the considered plane, which the colormap represents the E_z-component for the quasi-BIC modes, and the E_x-component for the GMR. By analyzing the individual field profiles and their spatial distribution, we notice several notable characteristics of the resonances. Firstly and most importantly, we notice that for both classes of resonances, the optical field is largely concentrated in the nearfield of the silicon resonators and localized in the organic coating. We observe that the intensity of the optical field is highest at plane B. This characteristic ensures a high overlap factor Γ_c through a high spatial overlap between the optical mode with the active organic layer, whose refractive index is changed upon an applied driving voltage. Secondly, the field intensity decays rapidly away from the silicon nanopillars and becomes minimal at the location of the interdigitated array of electrodes. Consequently the latter does not affect significantly the linewidth of the resonances. Thirdly, we note that both resonances are excited with x-polarized light. However, the field distribution in the high-intensity nearfield of the resonators is z-polarised for quasi-BIC and x-polarized for GMR. Consequently, an efficient operation of the electro-optic modulator on the r_{33} component is ensured by placing the contact electrodes parallel to the x-axis for the quasi-BIC and parallel to the z-axis for the GMR.

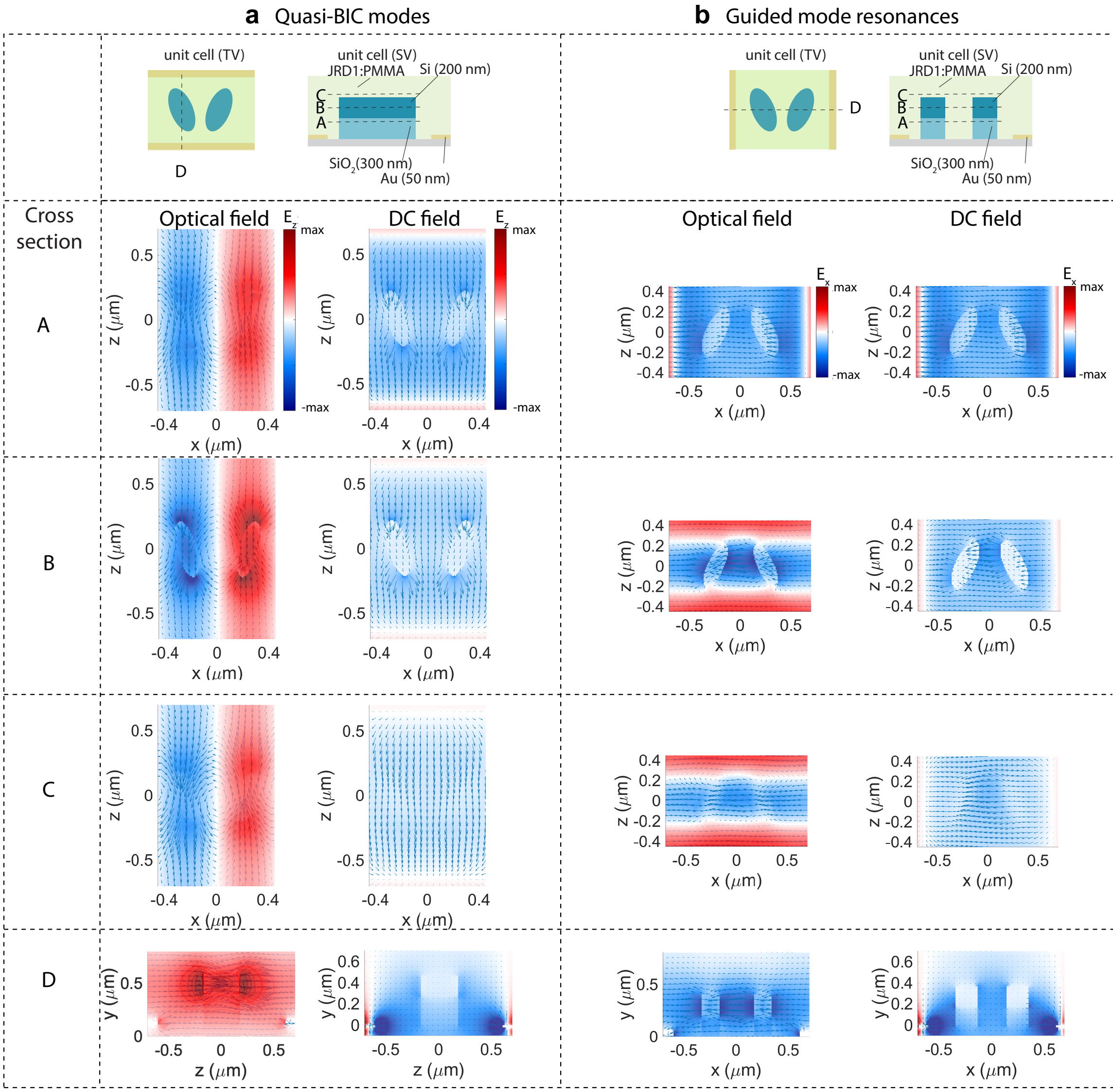

FIG. S2. **Optical and electro-static simulations.** Optical fields and DC fields of quasi-BIC modes (**a,**) and guided mode resonances (**b,**) under excitation with x-polarised light. The arrows indicate the in-plane orientation and relative magnitude of the plotted field while the colormap represents the E_z-component for quasi-BICs and E_x component for GMR (all planes A-D have the same range for the colorbar for all optical/electrostatic simulations of the quasi-BIC/GMR structures). Both classes of resonances are characterised by an optical field that is largely concentrated in the nearfield of the silicon resonators and localized in the active organic coating. The intensity of the optical field decays rapidly away from the silicon resonators. The optical mode is highly susceptible to refractive index changes in the nonlinear material, leading to the large observed tuning of its resonant wavelength. DC fields of quasi-BIC modes (**a,**) and guided mode resonances (**b,**) are indicative of the local orientation and level of alignment of the organic molecules with the poling field lines inside the three-dimensional volume of the organic layer. TV = top view, SV = side view.

83 The electrodes are then employed to establish the orientation of the electro-optic tensor

with respect to the geometrical coordinate system of the sample and thus the r_{33} electro-optic coefficient. r_{33} corresponds, by definition, to the direction of the electric field lines of the poling field. To visualize the latter, we provide in Fig. S2 also the electrostatic simulations of a DC field upon an applied voltage for all discussed planes A-D. We find that, as expected, the field amplitude decays far away from the electrodes and as a result, both the local r_{33} coefficient and the total introduced refractive index change Δn will be lower at plane C than at plane A. Finally, we underline two important last aspects. First, while the quasi-BIC optical mode is circulating, the GMR mode is mainly linearly polarised, thereby leading to a larger overlap factor with the r_{33} component for the GMR mode and the larger tuning of the resonant wavelength $\Delta\lambda_{res}$ for the GMR. Secondly, because of the high-Q nature of the quasi-BIC modes, an optimal height for the silicon dioxide pedestal was found experimentally to be at 300 nm to ensure at the same time a narrow-band resonance and a large electro-optic tuning at given applied voltage. Increasing the pedestal height would require higher tuning fields to achieve a commensurate effect due to the decay of the poling field as a function of height.

As discussed extensively in reference [2], the linewidth and the associated radiative Q-factor of the quasi-BIC resonances is directly linked with the asymmetry angle θ. In Fig. S3 we report this characteristic for the two geometric scaling parameters discussed in this study, $\alpha = 0.7$ and $\alpha = 0.725$. We find that at an angle of $\theta = 15°$ and $\alpha = 0.725$, the simulated Q-factor is around $Q_{sim} = 780$, higher than the experimental Q-factor of $Q = 550$. This discrepancy originates most probably from losses in the metallic structures. Also, owing to the losses present in the system, at small asymmetry angles θ, the visibility of the resonances is reduced.

Moreover, also the phase modulation introduced by the resonances depends strongly on the angle θ and the losses present in the system. In Fig. S4, we compare two sets of simulated transmission and phase with and without gold electrodes for a pedestal height of 300 nm and $\alpha = 0.725$. We clearly identify that even in the presence of gold electrodes, a phase modulation of about 35° is ocuring around the resonance. in the absence of gold electrodes, the quality factor is higher and the phase modulation stronger, about 100°.

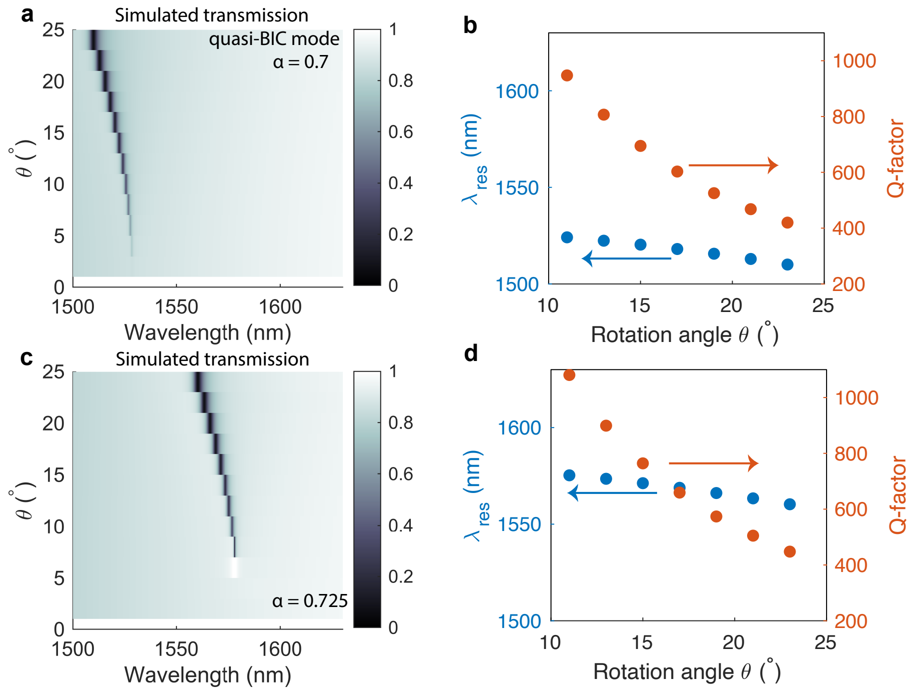

FIG. S3. **Linewidth tuning by angle θ.** Owing to the presence of material losses introduced by the metallic electrodes and the JRD1:PMMA layer, the visibility of resonances vanishes for small θ. **a,-b,** The geometrical scaling factor is $\alpha = 0.7$ and dimensions are as given in the methods. **c,-d,** The geometrical scaling factor is $\alpha = 0.725$. We compute the quality factor using the formula $Q = \frac{\omega_{res}}{\gamma}$ with γ the total loss rate of the resonance which we extract by fitting a Lorentzian lineshape to the transmitted power of the shape $I(\omega) = \frac{A}{(\omega-\omega_{res})^2+(\frac{\gamma}{2})^2} + B$, where A, B, ω_{res} and γ are fitting parameters.

S3. HIGH FREQUENCY CHARACTERISATION SETUP

We built an optical setup that is suited to characterise the samples both electrically and electro-optically at microwave frequencies. In Fig. S5 we show pictures of the real setup, featuring the characterization of the samples in transmission. The path taken by the telecom laser light is shown by the red arrows. Microwave GSG probes inject the modulation fields via complanar on-chip waveguides. They are positioned using xyz-stages. A fiber-coupled photodiode collects the transmitted light and the photocurrent signal is sent further to the set of mixers as described in the Methods in the main text. An InGaAs camera can be alternatively used to image and optimize the transmission of the telecom light through the modulator.

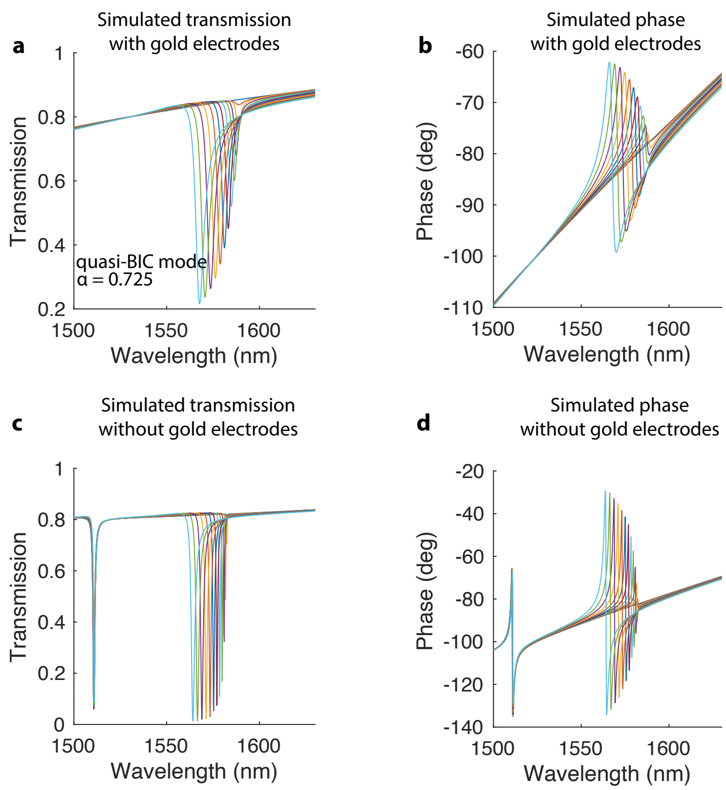

FIG. S4. **Phase and transmission tuning by angle θ. a,** The geometrical scaling factor is $\alpha = 0.725$ and gold electrodes are present. **b,** The geometrical scaling factor is $\alpha = 0.725$ and gold electrodes are missing.

---

[1] Ileana-Cristina Benea-Chelmus, Maryna Meretska, Delwin L. Elder, Michele Tamagnone, Larry R. Dalton, and Federico Capasso, "Electro-optic spatial light modulator from an engineered organic layer," in review (2021).

[2] Kirill Koshelev, Sergey Lepeshov, Mingkai Liu, Andrey Bogdanov, and Yuri Kivshar, "Asymmetric Metasurfaces with High- Q Resonances Governed by Bound States in the Continuum," Physical Review Letters **121**, 193903 (2018), arXiv:1809.00330.

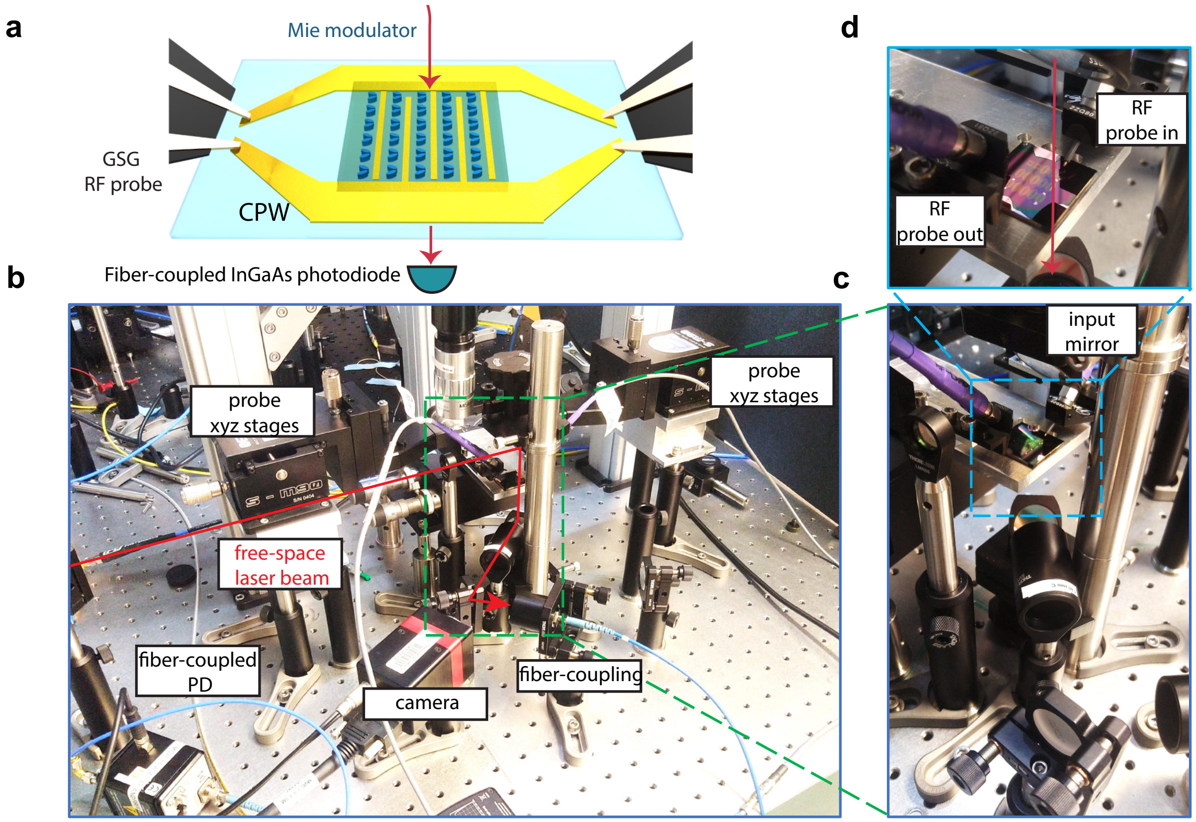

FIG. S5. **Pictures showing the GHz-speed setup used for electronic and electro-optic characterization of the Mie modulators.** **a,** Simplified setup sketch. **b,-d,** Photograph of setup shows free-space coupling of telecom light to the metasurface, GSG probes connected to the devices as well as fiber-coupled high-speed InGaAs detector. PD = photodiode, CPW = coplanar waveguides.